Verification of Anderson Superexchange in MnO via Magnetic Pair Distribution Function Analysis and *ab initio* Theory

Benjamin A. Frandsen,[1] Michela Brunelli,[2] Katharine Page,[3] Yasutomo J. Uemura,[1] Julie B. Staunton,[4] and Simon J. L. Billinge[5,6,*]

[1]*Department of Physics, Columbia University, New York, New York 10027, USA*
[2]*Swiss Norwegian Beamlines, European Synchrotron Radiation Facility (ESRF), 38000 Grenoble, France*
[3]*Spallation Neutron Source, Oak Ridge National Laboratory, Oak Ridge, Tennessee 37831, USA*
[4]*Department of Physics, University of Warwick, Coventry CV4 7AL, United Kingdom*
[5]*Condensed Matter Physics and Materials Science Department, Brookhaven National Laboratory, Upton, New York 11973, USA*
[6]*Department of Applied Physics and Applied Mathematics, Columbia University, New York, New York 10027, USA*

(Received 30 December 2015; published 11 May 2016)

We present a temperature-dependent atomic and magnetic pair distribution function (PDF) analysis of neutron total scattering measurements of antiferromagnetic MnO, an archetypal strongly correlated transition-metal oxide. The known antiferromagnetic ground-state structure fits the low-temperature data closely with refined parameters that agree with conventional techniques, confirming the reliability of the newly developed magnetic PDF method. The measurements performed in the paramagnetic phase reveal significant short-range magnetic correlations on a $\sim$1 nm length scale that differ substantially from the low-temperature long-range spin arrangement. *Ab initio* calculations using a self-interaction-corrected local spin density approximation of density functional theory predict magnetic interactions dominated by Anderson superexchange and reproduce the measured short-range magnetic correlations to a high degree of accuracy. Further calculations simulating an additional contribution from a direct exchange interaction show much worse agreement with the data. The Anderson superexchange model for MnO is thus verified by experimentation and confirmed by *ab initio* theory.

DOI: 10.1103/PhysRevLett.116.197204

Magnetic monoxide MnO, because of its relative simplicity, is often used as a benchmark system for the development of theoretical methods for understanding properties of transition metal oxides [1]. For example, various tight-binding models [2–4] and many important implementations of density functional theory (DFT) [5–10] that include the effects of strong electron correlations have been tested against MnO. Modern applications of these *ab initio* methods can successfully determine gross features of MnO, including the average atomic structure, magnetic ordering temperature, and local magnetic moment size. Unfortunately, efforts to draw conclusions about the underlying physics from these computations are frequently complicated by the fact that differing theories often rely on significantly different assumptions and make widely varying predictions about important details of the system. Among others, these details include the precise orientation of the magnetic moments in the antiferromagnetic (AF) phase, the nature of the short-range magnetic correlations above T_N, and the mechanism(s) for magnetic exchange.

Experimental techniques capable of probing local structure and properties can address these issues in ways not possible with bulk probes of average properties. Illustrating this are recent neutron total scattering experiments [11,12] that revealed a previously hidden local monoclinic distortion in MnO at low temperature and a preferred spin orientation axis along $[10\bar{1}]$ or $[11\bar{2}]$. This new information, inaccessible by standard characterization techniques such as magnetic susceptibility and conventional neutron diffraction, can then be used to differentiate between competing theories. In this Letter, we utilize magnetic pair distribution function (mPDF) analysis [13], a recently developed method for investigating local magnetic structure, to measure directly the short-range magnetic correlations in the paramagnetic state of MnO from temperature-dependent neutron total scattering experiments. We use these results to evaluate competing theories of magnetic exchange in MnO, finding that the Anderson superexchange [1] obtained from recent DFT calculations with the self-interaction-corrected (SIC) local spin density approximation [14,15] in the "disordered local moment" (DLM) approach [16,17] describes the data exceptionally well with no need for an additional direct exchange contribution present in other models. In addition to resolving this long-standing question about MnO, this work highlights the mPDF technique and the DLM-DFT(+SIC) scheme as valuable tools for studying the magnetic properties of strongly correlated electron systems.

Neutron time-of-flight total scattering measurements were performed at the NPDF instrument at the spallation source located at the Lujan Neutron Scattering Center at Los Alamos National Laboratory on a commercial sample of MnO (Alfa Aesar, 99% pure). Low backgrounds and wide momentum-transfer coverage contributed to

high-quality data appropriate for magnetic and atomic pair distribution function (PDF) analysis. The data were reduced for PDF transformation according to standard protocols within the program PDFGETN [18]. A closed cycle refrigerator was used to access temperatures between 15 and 300 K. We also conducted neutron scattering measurements on the same sample at the D20 instrument of the Institute Laue-Langevin (ILL) reactor source, using a neutron wavelength of 0.94079 Å and an orange cryostat for temperatures in the range $5 < T < 300$ K.

Similar to the atomic PDF [19], the mPDF technique involves normalizing and Fourier transforming the magnetic scattering intensity from a powder sample to obtain the pairwise magnetic correlation function directly in real space. Because both Bragg and diffuse scattering are included, the mPDF is sensitive to both long- and short-range magnetic correlations. Simplistically speaking, pairs of spins with parallel alignment contribute a positive peak in the mPDF and antiparallel spins give a negative peak, providing a highly intuitive view of spin correlations on a local length scale. The full definition of the mPDF equations is in Ref. [13].

In practice, the mPDF is most easily obtained when it is done simultaneously with the atomic PDF $G(r)$ [12], without separating the magnetic and nuclear scattering signals or normalizing the magnetic scattering by the magnetic form factor, $f_m(Q)$ as originally proposed [13]. The unnormalized mPDF quantity $d(r)$ obtained this way is given by [12]

$$d(r) = C_1 \times f(r) \circ S(r) + C_2 \times \frac{dS}{dr}, \qquad (1)$$

where $f(r)$ is the properly normalized mPDF derived in Ref. [13], C_1 and C_2 are constants related by $C_1/C_2 = -1/\sqrt{2\pi}$ when the ordered moment is fully saturated (the ratio is smaller in magnitude otherwise), $\circ$ represents the convolution operation, and $S(r) = \mathcal{F}\{f_m(Q)\} \circ \mathcal{F}\{f_m(Q)\}$, where $\mathcal{F}\{\square\}$ denotes the Fourier transform. The second term in this equation, which appears as a peak at very low r, contains no information about magnetic correlations and is determined entirely by the spatial distribution of the localized Mn^{2+} magnetic moment. This equation provides a straightforward method to calculate $d(r)$ from a magnetic structure model for direct comparison with the experimental mPDF and has been implemented as an extension to the Diffpy-CMI software package [20], and this approach to modeling the mPDF was used in the current work.

Figure 1 displays the combined atomic and magnetic PDFs obtained from the NPDF instrument at three representative temperatures: 15 (deep in the ordered state), 100, and 120 K (just above the AF transition at $T_N = 118$ K). For each temperature, we first refined the rhombohedral structural model and then used the residual after subtraction of the calculated $G(r)$ to refine the magnetic structure, modeled by the known long-range type-II antiferromagnetic structure

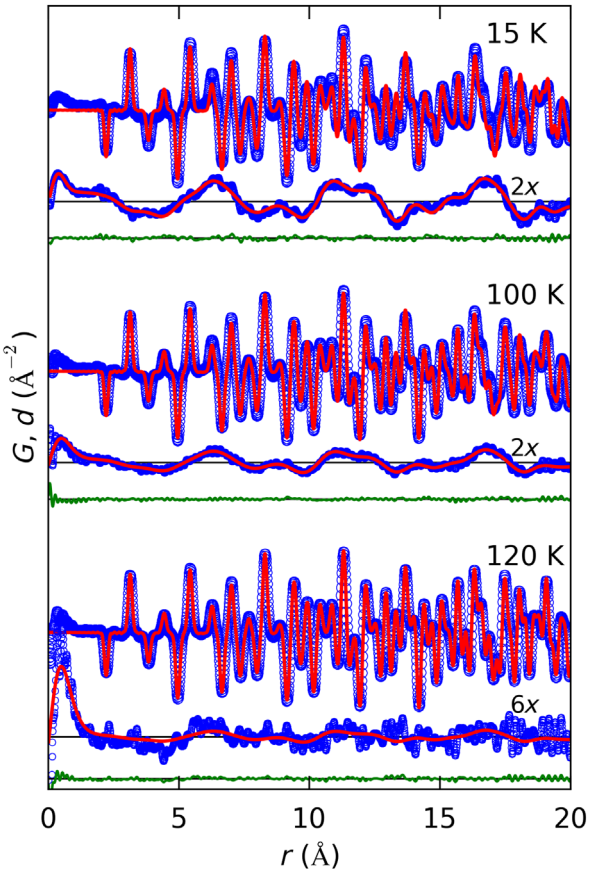

FIG. 1. Combined atomic and magnetic PDFs of MnO at representative temperatures. For each temperature, the combined atomic and magnetic PDF is shown as the top blue curve, with the refined atomic PDF overlaid in red; the residual from the atomic PDF fit is shown as the lower blue curve, with the refined mPDF overlaid in red (both magnified by the factor indicated for clarity); and the green curve gives the overall fit residual.

and constrained by the atomic positions from the structural fit. This magnetic structure consists of ferromagnetically aligned spins within common (111) sheets and antiferromagnetic coupling between adjacent sheets. All fits were performed from 0 to 20 Å. For each temperature, the top set of curves shows in blue the total experimental PDF (structural and magnetic) and in red the refined structure-only PDF $G(r)$; the second set shows in blue the residual signal after subtraction of the calculated $G(r)$ and in red the refined mPDF $d(r)$ (magnified for clarity as indicated in the figure); and the lower green curve shows the combined PDF + mPDF fit residual, revealing an excellent overall fit quality. Although previous work [11,12] demonstrated that the local structure at low temperature has a slight monoclinic distortion, we use the rhombohedral model at all temperatures for simplicity. Interestingly, our structural refinements with the rhombohedral model indicate that a slight rhombohedral distortion persists on a ~5–10 nm length scale in the high-temperature cubic phase. Details of this local distortion are provided in the Supplemental Material [21].

The mPDF signal can be easily distinguished from the atomic PDF by two features: it is lower in frequency and characteristically broader than the atomic PDF due to the effects of the magnetic form factor, and it changes more dramatically with temperature. This allows for robust refinement of the atomic and magnetic structures with no risk of confounding the fits. We noticed that the mPDF peak at low r arising from the second term in Eq. (1) is rather independent of temperature, as expected when the local moment size and spatial distribution are constant, so we performed a global fit to this feature at all temperatures to determine C_2, which we fixed for subsequent analysis. Imposing the known long-range AF structure of MnO left the scale factor C_1 as the only free parameter in our mPDF fits. This scale factor is proportional to the square of the ordered magnetic moment, similar to the intensity of a magnetic Bragg peak for long-range magnetic order. In Fig. 2, we plot $\sqrt{C_1}$ as a function of temperature (normalized by its maximum value) as red dots and compare it to the normalized magnetic order parameter determined by the precession frequency in a muon spin rotation (μSR) experiment [22], the square root of the maximum intensity of the first AF Bragg peak obtained from our ILL reactor source measurements, and the square root of the integrated intensity of the same AF Bragg peak from the total scattering structure function $S(Q)$ of the time-of-flight neutron data. The results from these approaches mutually confirm each other by their close agreement below T_N and demonstrate the reliability of the mPDF approach for analyzing magnetic scattering data.

More interesting is the behavior of the mPDF scale factor above T_N: we observe that $\sqrt{C_1}$ remains finite but decays approximately exponentially with temperature above T_N,

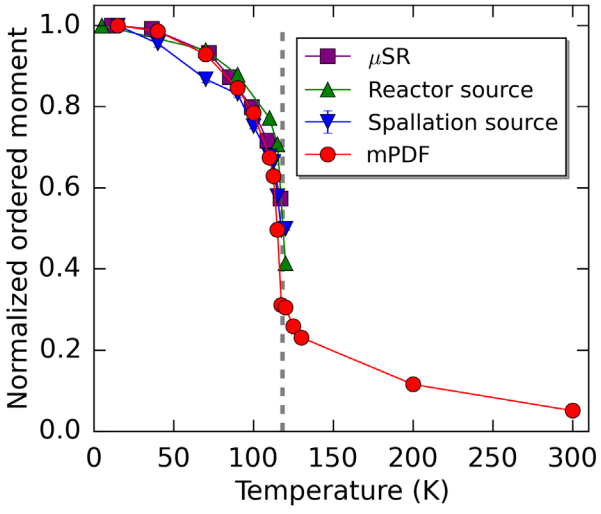

FIG. 2. Magnetic order parameter obtained from different experimental techniques, including the μSR precession frequency, the maximum AF Bragg peak intensity from a reactor source, the integrated AF Bragg peak intensity from a spallation source, and the refined mPDF fit of the known magnetic structure of MnO at low temperature. The vertical dashed line indicates the magnetic ordering temperature of 118 K.

confirming the presence of short-range magnetic correlations in the paramagnetic state. This in itself provides no new information since the existence of short-range magnetic correlations can already be inferred from the presence of a small but visible hump of diffuse scattering near where the first AF Bragg peak appears at lower temperature [23–25]. The unique contribution of the mPDF analysis becomes more apparent with a close inspection of the mPDF fits above T_N, which reveal that the long-range type-II AF structure does not actually fit the mPDF data well, particularly for the first few nearest neighbors. For example, the experimental mPDF peaks associated with the second- and fourth-nearest-neighbor spin pairs near 4.4 and 6.3 Å are consistently much higher in magnitude than predicted by the long-range structure, as seen for the 120 K fit in Fig. 1. This indicates that the short-range magnetic correlations in the paramagnetic phase deviate significantly from the long-range structure and cannot be viewed simply as the same type of magnetic order on a weaker or shorter length scale. These subtle differences can provide important insights into the underlying physics and may help differentiate competing theories.

To pursue this further, we turned to the disordered local moment DLM-DFT of finite-temperature magnetism [16] in which strong electronic correlations evident in transition metal oxides [17] and lanthanide compounds [26,27], for example, are treated with the self-interaction correction [15]. When applied to MnO, the theory accounts for the magnitude of the insulating gap and its persistence into the paramagnetic phase, the magnetic ordering temperature and the onset of the type-II AF state. Our first-principles DLM-DFT calculations find the ground-state Mn-ion configuration to be Mn^{2+} with five localized d states constituting a half-filled shell in line with Hund's first rule.

Without prior assumption of any specific effective spin Hamiltonian, the key quantity calculated by DLM-DFT is the lattice Fourier transform (LFT), $\mathcal{S}^{(2)}(\mathbf{q})$, of the direct correlation function $\mathcal{S}^{(2)}_{0n}$ for the local Mn moments, from which the magnetic correlation function, $\langle \mathbf{S}_0 \cdot \mathbf{S}_n \rangle$, can be determined. Here, $\mathbf{S}_0$ represents a classical Heisenberg spinlike local moment arbitrarily chosen to be at the origin, $\mathbf{S}_n$ represents a spin in the nth coordination shell (assuming the ideal cubic structure), and the angled brackets denote an average over all of the spins in that shell. We find the $\langle \mathbf{S}_0 \cdot \mathbf{S}_n \rangle$'s using an Onsager cavity field calculation [28] by solving the coupled integral equations, $C(\mathbf{q})^{-1} = [1 - \beta(\mathcal{S}^{(2)}(\mathbf{q}) - \Lambda)]$ and $\Lambda = \int \mathcal{S}^{(2)}(\mathbf{q}) C(\mathbf{q}) d\mathbf{q}$ for the LFT of the magnetic correlation function, $C(\mathbf{q})$This pair of equations ensures that the sum rule $\langle S_0^2 \rangle = 1$ is met Furthermore, the real space $\mathcal{S}^{(2)}_{0n}$ quantities describe the magnetic exchange interactions, the J_n's, between the Mn spins on different shells. When analyzed in concert with the underlying electronic structure [17], an *ab initio* prediction of a "textbook" picture of Anderson superexchange between O $2p$ and Mn $3d$ orbitals emerges.

In Fig. 3, we display the magnetic correlation functions $\langle \mathbf{S}_0 \cdot \mathbf{S}_n \rangle$ calculated as a function of temperature from the

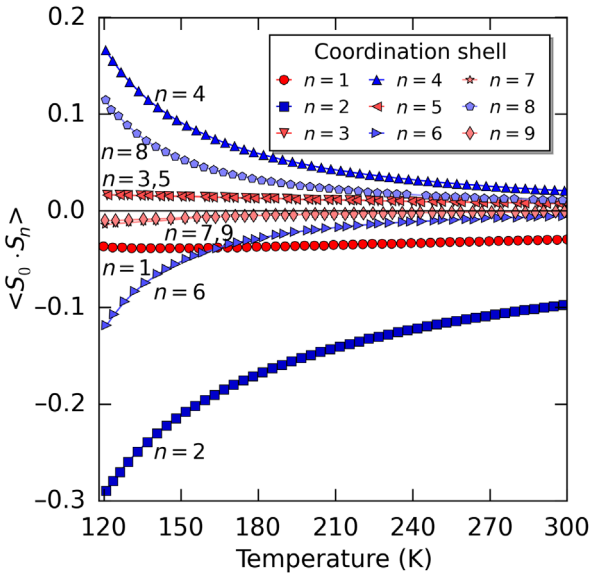

FIG. 3. Temperature-dependent magnetic correlation functions of MnO for the first nine nearest neighbors of the cubic structure calculated from the *ab initio* theory described in the text.

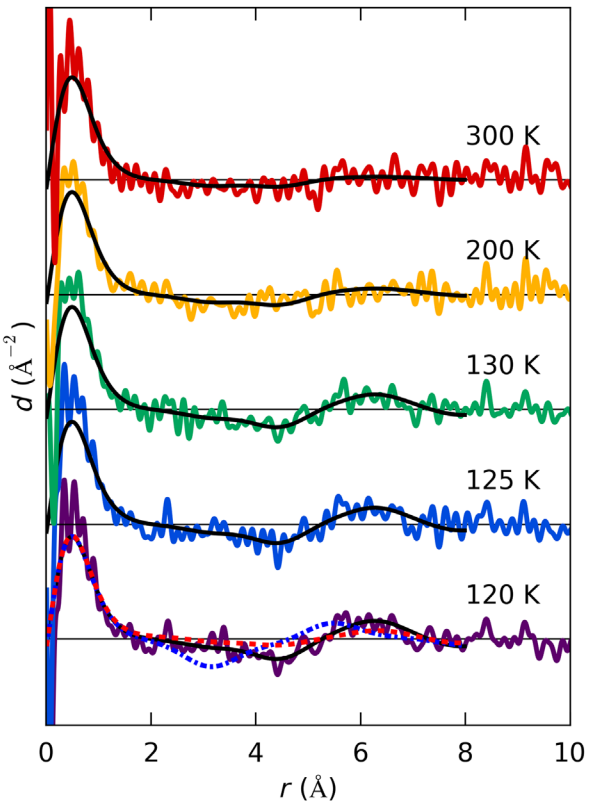

FIG. 4. Experimental (thick colored curves) and calculated (thinner black curves) mPDFs of MnO at five temperatures in the paramagnetic state. For 120 K, the best fit of the low-temperature long-range-ordered structure is shown as a dashed red curve, and the calculated mPDF for a larger J_1/J_2 ratio simulating a direct exchange scenario is shown as the blue dash-dotted line.

ab initio theory. The *ab initio* calculations were done in terms of the dimensionless temperature ratio T/T_N, which we converted to a physical temperature using the known T_N of 118 K. It is notable that the magnetic correlations with odd-numbered shells, shown in red hues, are significantly smaller (though more independent of temperature) than those with even-numbered shells (blue hues). This reflects the geometric frustration of the type-II AF structure on the face-centered-cubic Mn sublattice, in which half of the neighbors in the odd-numbered shells lie within the same (111) plane as the central spin $\mathbf{S}_0$ and would therefore tend to be parallel to it, while the other half are in planes with opposite magnetization in the ordered state. In contrast, the neighbors in even-numbered shells suffer no such frustration and can all have a uniform tendency for either parallel or antiparallel alignment with the central spin.

To compare the theory to the experiment, we calculated the individual mPDF contributions from a cubic model of the first nine near-neighbor coordination shells determined by atomic PDF fits and scaled them according to the predicted correlation function at the appropriate temperature. The results of this procedure are displayed for the five measurements obtained in the paramagnetic state in Fig. 4. The calculated mPDF functions are shown as black solid curves overlaid on the data. The agreement between theory and experiment is excellent at all temperatures, especially considering that there are no free parameters in these calculations. For comparison, the best fit of the long-range magnetic structure is shown for 120 K as the red dashed curve. It clearly describes the data much worse than the *ab initio* prediction, particularly for the second- and fourth-nearest neighbors at ~4.4 and ~6.3 Å. These experimental results are in general agreement with earlier magnetic reverse Monte Carlo analysis of MnO [25]. Further details regarding the structural and magnetic PDF refinements and calculations are found in the Supplemental Material [21].

The mPDF data allow us to compare different *ab initio* theories. A common difference among *ab initio* theories is the first- and second-nearest-neighbor exchange parameter ratio J_1/J_2, which can vary widely from more than 3.5 to less than 0.4 (see, e.g., Table III in Ref. [6]). The present DLM-DFT method, producing essentially Anderson superexchange, predicts $J_1/J_2 = 0.502$. Higher ratios, such as 3.571, given by recent tight-binding calculations [4], are typically reflective of a substantial Mn-Mn direct exchange contribution in addition to the superexchange. The calculated temperature-dependent correlation functions can easily be modified to reflect different J_1/J_2 ratios, from which the mPDF can be generated and compared to the experiment. We show the result for $J_1/J_2 = 2.0$ at 120 K as the blue dash-dotted curve in Fig. 4. Unsurprisingly, the larger ratio leads to stronger nearest-neighbor correlations, causing the calculated mPDF to differ significantly from the data. The fits suggest that the J_1/J_2 ratio is smaller, and close to 0.5, which supports a picture of there being Anderson superexchange without any significant contribution from direct exchange.

To be more quantitative, we calculated the mPDF at the five temperatures above T_N for 17 different J_1/J_2 ratios distributed on the interval [0,1.2]. For each combination of temperature and exchange ratio, we calculated the summed squared difference between data and calculation (χ^2). We then fit a parabola to the 17 (J_1/J_2, χ^2) ordered pairs for each temperature, with a common parabolic minimum refined as a global parameter to obtain the best-fit value of J_1/J_2. We took care to properly weight with the statistical uncertainties on the data propagated from the original PDF on the Nyquist grid [29]. Details are available in the Supplemental Material [21]. This procedure revealed an optimal exchange ratio of $J_1/J_2 = 0.67 \pm 0.12$, in fairly close agreement with the predicted value from DLM-DFT and well away from larger values indicative of significant direct exchange contributions. This increases our confidence in the superexchange-dominated picture obtained from the DLM-DFT approach. Although experimental estimates of J_1/J_2 are few in number and vary from significantly less than 1 to well over 2, most place J_1/J_2 in the range of 0.8–0.9, in relatively good agreement with the present results [30–33].

These findings constitute experimental and theoretical verification of the Anderson superexchange model of magnetic interactions in MnO. The success of the DLM-DFT *ab initio* scheme for MnO suggests that it should be a good starting point for other transition-metal oxides and, coupled with measurement techniques such as mPDF, will be of significant utility for understanding more complex materials. We have also demonstrated that the mPDF method can yield unique insights into magnetic systems by allowing for a quantitative analysis of short-range magnetic correlations directly in real space. We expect this to be valuable in the study of strongly correlated systems and other materials known to have short-range magnetism.

We thank Joan Siewenie for the technical assistance with the measurements performed on the NPDF instrument. B. A. F. and Y. J. U. acknowledge support from the NSF via PIRE Program No. OISE-0968226 and DMREF Program No. DMR-1436095, and B. A. F. by NSF GRFP Program No. DGE-11-44155. S. J. L. B. acknowledges support from the U.S. Department of Energy, Office of Science, Office of Basic Energy Sciences (DOE-BES) under Contract No. DE-SC00112704. J. B. S. acknowledges support from EPSRC (UK) Grant No. EP/J006750/1. Neutron scattering experiments were carried out on NPDF at the Lujan Center, funded by the DOE Office of Basic Energy Sciences. LANL is operated by Los Alamos National Security LLC under DOE Contract No. DE-AC52-06NA25396.

*sb2896@columbia.edu

[1] P. W. Anderson, Phys. Rev. **115**, 2 (1959).
[2] M. Takahashi and J.-i. Igarashi, Phys. Rev. B **54**, 13566 (1996).
[3] W. A. Harrison, Phys. Rev. B **76**, 054417 (2007).
[4] W. A. Harrison, Phys. Rev. B **77**, 245103 (2008).
[5] J. E. Pask, D. J. Singh, I. I. Mazin, C. S. Hellberg, and J. Kortus, Phys. Rev. B **64**, 024403 (2001).
[6] G. Fischer, M. Däne, A. Ernst, P. Bruno, M. Lüders, Z. Szotek, W. Temmerman, and W. Hergert, Phys. Rev. B **80**, 014408 (2009).
[7] F. Tran and P. Blaha, Phys. Rev. Lett. **102**, 226401 (2009).
[8] P. Thunström, I. Di Marco, and O. Eriksson, Phys. Rev. Lett. **109**, 186401 (2012).
[9] R. Sakuma and F. Aryasetiawan, Phys. Rev. B **87**, 165118 (2013).
[10] S. Das, J. E. Coulter, and E. Manousakis, Phys. Rev. B **91**, 115105 (2015).
[11] A. L. Goodwin, M. G. Tucker, M. T. Dove, and D. A. Keen, Phys. Rev. Lett. **96**, 047209 (2006).
[12] B. A. Frandsen and S. J. L. Billinge, Acta Crystallogr. Sect. A **71**, 325 (2015).
[13] B. A. Frandsen, X. Yang, and S. J. L. Billinge, Acta Crystallogr. Sect. A **70**, 3 (2014).
[14] J. P. Perdew and A. Zunger, Phys. Rev. B **23**, 5048 (1981).
[15] M. Lüders, A. Ernst, M. Däne, Z. Szotek, A. Svane, D. Ködderitzsch, W. Hergert, B. L. Györffy, and W. M. Temmerman, Phys. Rev. B **71**, 205109 (2005).
[16] B. L. Gyorffy, A. J. Pindor, J. Staunton, G. M. Stocks, and H. Winter, J. Phys. F **15**, 1337 (1985).
[17] I. D. Hughes, M. Däne, A. Ernst, W. Hergert, M. Lüders, J. B. Staunton, Z. Szotek, and W. M. Temmerman, New J. Phys. **10**, 063010 (2008).
[18] P. F. Peterson, M. Gutmann, T. Proffen, and S. J. L. Billinge, J. Appl. Crystallogr. **33**, 1192 (2000).
[19] T. Egami and S. J. L. Billinge, *Underneath the Bragg Peaks: Structural Analysis of Complex Materials*, 2nd ed. (Elsevier, Amsterdam, 2012).
[20] P. Juhás, C. L. Farrow, X. Yang, K. R. Knox, and S. J. L. Billinge, Acta Crystallogr. Sect. A **71**, 562 (2015).
[21] See Supplemental Material at http://link.aps.org/supplemental/10.1103/PhysRevLett.116.197204 for details about the structural and magnetic PDF refinements, determination of the optimal exchange parameter ratio, and discussion of the robustness of the mPDF signal.
[22] Y. J. Uemura, T. Yamazaki, Y. Kitaoka, M. Takigawa, and H. Yasuoka, Hyperfine Interact. **17**, 339 (1984).
[23] C. G. Shull, W. A. Strauser, and E. O. Wollan, Phys. Rev. **83**, 333 (1951).
[24] I. A. Blech and B. L. Averbach, Physics **1**, 31 (1964).
[25] A. Mellergård, R. McGreevy, A. Wannberg, and B. Trostell, J. Phys. Condens. Matter **10**, 9401 (1998).
[26] I. D. Hughes, M. Däne, A. Ernst, W. Hergert, M. Lüders, J. Poulter, J. B. Staunton, A. Svane, Z. Szotek, and W. M. Temmerman, Nature (London) **446**, 650 (2007).
[27] L. Petit, D. Paudyal, Y. Mudryk, K. A. Gschneidner, V. K. Pecharsky, M. Lüders, Z. Szotek, R. Banerjee, and J. B. Staunton, Phys. Rev. Lett. **115**, 207201 (2015).
[28] J. B. Staunton and B. L. Gyorffy, Phys. Rev. Lett. **69**, 371 (1992).
[29] C. L. Farrow, M. Shaw, H.-J. Kim, P. Juhás, and S. J. L. Billinge, Phys. Rev. B **84**, 134105 (2011).
[30] M. E. Lines and E. D. Jones, Phys. Rev. **139**, A1313 (1965).
[31] M. Kohgi, Y. Ishikawa, and Y. Endoh, Solid State Commun. **11**, 391 (1972).
[32] D. Bloch and R. Maury, Phys. Rev. B **7**, 4883 (1973).
[33] G. Pepy, J. Phys. Chem. Solids **35**, 433 (1974).